RSC Advances

PAPER

View Article Online
View Journal | View Issue

Cite this: *RSC Adv.*, 2024, **14**, 23560

Mesoporous Fe_3O_4/SiO_2/poly(2-carboxyethyl acrylate) composite polymer particles for pH-responsive loading and targeted release of bioactive molecules†

Most. Nusrat Jahan,[a] Md. Ashraful Alam,[a] Md. Mahabur Rahman,[ab] S. Manjura Hoque [c] and Hasan Ahmad *[a]

pH-responsive polymer microspheres undergoing reversible changes in their surface properties have been proved useful for drug delivery to targeted sites. This paper is aimed at preparing pH-responsive polymer-modified magnetic mesoporous SiO_2 particles. First, mesoporous magnetic (Fe_3O_4) core-particles are prepared using a one-pot solvothermal method. Then, magnetic Fe_3O_4 particles are covered with a C=C functional mesoporous SiO_2 layer before seeded emulsion polymerization of 2-carboxyethyl acrylate (2-CEA). The composite polymer particles are named Fe_3O_4/SiO_2/P(2-CEA). The average diameters of the Fe_3O_4 core and Fe_3O_4/SiO_2/P(2-CEA) composite polymer particles are 414 and 595 nm, respectively. The mesoporous (pore diameter = 3.41 nm) structure of Fe_3O_4/SiO_2/P(2-CEA) composite polymer particles is confirmed from Brunauer–Emmett–Teller (BET) surface analysis. The synthesized Fe_3O_4/SiO_2/P(2-CEA) composite polymer exhibited pH-dependent changes in volume and surface charge density due to deprotonation of the carboxyl group under alkaline pH conditions. The change in the surface properties of Fe_3O_4/SiO_2/P(2-CEA) composite polymer particles following pH change is confirmed from the pH-dependent sorption of cationic methylene blue (MB) and anionic methyl orange (MO) dye molecules. The opening of the pH-responsive P(2-CEA) gate valve at pH 10.0 allowed the release of loaded vancomycin up to 99% after 165 min and *p*-acetamido phenol (*p*-AP) up to 46% after 225 min. Comparatively, the amount of release is lower at pH 8.0 but still suitable for drug delivery applications. These results suggested that the mesoporous Fe_3O_4/SiO_2 composite seed acted as a microcapsule, while P(2-CEA) functioned as a gate valve across the porous channel. The prepared composite polymer can therefore be useful for treating intestine/colon cancer, where the pH is comparatively alkaline.

Received 29th April 2024
Accepted 12th July 2024

DOI: 10.1039/d4ra03160a

rsc.li/rsc-advances

1. Introduction

In the current era, researchers have concentrated on developing drug delivery systems (DDSs) that are structurally robust and capable of transporting significant amounts of drug molecules to specific tissues or even within organelles without the risk of premature release. Many drugs such as anticancer drugs are not selective in nature. They cannot distinguish between healthy cells and cancer-affected cells. Hence, after oral intake, they can affect healthy cells and may also be disintegrated by stomach acid during their passage to the intestine. To overcome these problems, smart DDSs are needed. Porous materials with well-defined structures have attracted significant attention owing to their large surface area and confined pore space available for accommodating active drugs, which in turn increases their ability to interact with neighboring affected cells through the release of drugs. These porous substances also have promising usability in adsorption, separation, catalysis, drug administration, purification, chemical sensing, energy conversion and storage.[1–9] Different types of porous materials such as SiO_2,[1,2] metal oxides,[1,10] carbon,[1,11] graphene,[12] polymers,[1,3] zeolite,[1,13] silver,[14] and gold,[15] are available in the literature. Among these, mesoporous SiO_2 particles are attracting significant interest as drug carriers.[16–18] This is owing to their interesting characteristics, including a large surface area, well-defined pore structures with a high pore volume, adjustable particle size, and a surface that can be easily modified (because of the abundance

[a]*Department of Chemistry, Research Laboratory of Polymer Colloids and Nanomaterials, Rajshahi University, Rajshahi 6205, Bangladesh. E-mail: samarhass@yahoo.com; hahmad@ru.ac.bd*

[b]*Department of Chemistry, Pabna University of Science and Technology, 6600 Pabna, Bangladesh*

[c]*Materials Science Division, Bangladesh Atomic Energy Commission, Dhaka, Bangladesh*

† Electronic supplementary information (ESI) available. See DOI: https://doi.org/10.1039/d4ra03160a

of silanol groups). Additionally, these particles possess excellent water dispersibility, chemical inertness, biocompatibility, and a high capacity for loading drugs.[19–21] DDSs have attracted growing interest owing to their ability to regulate the rate and/or site of drug release and their efficiency in enhancing drug efficacy, mitigating hazardous side effects, promoting drug adsorption and target site accessibility, and synchronizing the delivery of drugs in optimal time. Stimuli-responsive polymers play an essential role in achieving these therapeutic outcomes. These polymers exhibit responsiveness to variations in physical factors, such as temperature, light, ionic strength, solvents, radiation (UV, visible), mechanical stress, high pressure, sonic radiation, magnetic field and electrical field, as well as chemical factors such as pH, glucose concentration, and redox potential.[22–25] pH- and temperature-responsive polymers have gained attention in DDSs because they are common physiological parameters in human body. The polymeric materials, sensitive to pH, contain ionizable groups attached to their structure. These groups can undergo protonation or deprotonation in response to changes in the surrounding pH and release the drug from pH-sensitive DDSs.[26,27] To expand the potential applications of these materials, it is essential to fabricate them with a paramagnetic feature, which would allow for a wider range of uses, from separation to drug delivery. By applying an external magnetic field, it is possible to keep magnetic particles confined to a certain organ for a specific duration, preventing the particles from spreading throughout the entire circulatory system. The application potential of magnetic iron oxide particles is extensive, encompassing diverse areas such as controlled drug delivery,[28] DNA separation,[29] protein purification,[30] catalysis,[31] hyperthermia in tumor tissues,[32] and magnetic resonance imaging (MRI).[33] These magnetic particles can be readily manipulated by the application of an external magnetic field during use.

The present research is devoted to the modification of submicron-sized mesoporous magnetic Fe_3O_4/SiO_2 composite particles with anionic pH-responsive polymers for regulating the off- and on-capping of void channels, and the controlled release of encased drug molecules with changing pH value. This would prevent the premature release of toxic drug molecules, and thus could minimize the cell toxicity. So far, most research studies start with the preparation of magnetic mesoporous SiO_2 nanoparticles (Fe_3O_4/m-SiO_2) consisting of a solid magnetite core and a mesoporous SiO_2 shell. For example, Zhao *et al.* modified Fe_3O_4/m-SiO_2 with hydroxyapatite nanovalves for controlled release of the ibuprofen drug.[34] Tang and associates prepared a novel Fe_3O_4@m-SiO_2(DOX)@HSA(Ce6) nanoplatform for sustained release of DOX under acidic condition.[35] Here, polydopamine was used to block the mesoporous channels, and human serum albumin (HSA) was conjugated to increase the biocompatibility and provide a vehicle for loading chlorin e6 (Ce6). Recently, Lai *et al.* modified Fe_3O_4/m-SiO_2 composite microspheres with the copolymer of carboxymethyl chitosan (CMCS) and poly[2-(dimethylamino)ethyl methacrylate] (PDMA) to introduce pH-responsive functionality.[36] Keshavarz *et al.* reported modification of Fe_3O_4/m-SiO_2 nanoparticles with pH-responsive chitosan hydrogels, and studied the pH- and temperature-responsive drug release for applications in chemotherapy and hyperthermia.[37] Avedian *et al.* labeled Fe_3O_4/m-SiO_2 nanoparticles with poly(ethyleneimine)-conjugated folic acid, and studied the release profile of anticancer drugs at different pH values.[38] Zhao *et al.* designed Fe_3O_4/m-SiO_2 conjugated folic acid-linked chitosan microspheres as a redox and pH dual-responsive platform for magnetothermal therapy and chemotherapy.[39] Chang *et al.* studied the pH-responsive release of DOX from a dual pH- and thermo-responsive poly(*N*-isopropylacrylamide-*co*-methacrylic acid) (PNIPAM-*co*-MAA)-coated Fe_3O_4/m-SiO_2 microsphere.[40]

In these above research studies, the thin mesoporous SiO_2 shell around the solid magnetite nanosized core-particles seemed to be inadequate for housing a sufficient amount of drug molecules for magnetothermal therapy and chemotherapy treatments of cancer affected cells. So, the present investigation is concentrated on the preparation of sub-micrometer sized mesoporous Fe_3O_4 core-particles, followed by modification with the mesoporous SiO_2 shell, and then finally with the pH-responsive polymer valve. In a previous research study, we prepared mesoporous Fe_3O_4/SiO_2 composite particles and modified them with the P(NIPAM-DMA) copolymer.[41] The pH-responsive off- and on-capping, due to the protonation of the tertiary amine group of the PDMA moiety in the acidic environment, triggered the release of the loaded drug molecules. This type of microsphere was considered useful for treating cancer, as the microenvironment inside the solid tumors is acidic (pH 5–6.8).[42] Rather than cationic DMA, a new anionic 2-carboxyethyl acrylate (2-CEA) monomer has been used here to modify the mesoporous Fe_3O_4/SiO_2 composite seed particles and the composite polymer is named as Fe_3O_4/SiO_2/P(2-CEA). The preparation protocol is depicted in Scheme S1.† The deprotonation of carboxyl groups in poly(2-CEA) at the alkaline pH range would assist in the gate opening of the porous channel and facilitate the controlled release of loaded/encased drug molecules from the mesoporous Fe_3O_4/SiO_2 composite seed, acting as a microcapsule. Thus, the anionic poly(2-CEA) polymer would add stability to DDSs, preventing gastric degradation and the denaturation of loaded drugs at acidic pH (pH 1–3) while passing through the stomach, and subsequently release drugs to specific locations where the pH is alkaline, such as the upper small intestine and colon that are further inside the gastrointestinal tract.[43–45] It should be noted that the anionic 2-CEA monomer has rarely been used in DDSs, except in formulating adhesives, gel-casting agents for ceramic powder, and sorbent materials for waste water remediation.[46–49] The poly(2-CEA) is known for possessing enhanced mechanical and thermal properties, flexibility, and better physical bonding capacity with the metal surface.[46] These properties would favor the preparation of a stable Fe_3O_4/SiO_2/P(2-CEA) composite polymer latex for applications in smart DDSs. The water insolubility of poly(2-CEA) and its sole use for preparing DDSs would also help to achieve structural regularity in the polymer microstructure with viable and reproducible application property. In addition, the sub-micrometer size distribution and paramagnetic property of pH-responsive polymer gated mesoporous Fe_3O_4/SiO_2 composite particles could be beneficial for

use in the release of perfumes, agrochemicals, biocatalysis, water cleaning, photographic films, cell separation, hyperthermia and MRI.[41,50,51]

2. Experimental

2.1. Materials

The monomer grade 2-carboxyethyl acrylate (2-CEA), purchased from Sigma-Aldrich, USA, was purified by passing through a basic activated alumina column. Tetraethyl orthosilicate (TEOS), from Sigma-Aldrich Chemie GmbH, USA, was preserved in the refrigerator and utilized for the chemical modification of Fe_3O_4 core particles. Cetyltrimethyl ammonium bromide (CTAB), a cationic template from Fluka, Biochemica, Switzerland, was employed to create porosity. 3-(Trimethoxysilyl) propyl methacrylate (MPS) was obtained from Alfa Aesar, UK, and used to introduce vinyl functionality and to initiate free radical polymerization from the surface. The free radical water-soluble initiator, potassium persulfate (KPS), was procured from LOBA Chem., India, and recrystallized from distilled water before use. Ethylene glycol from Merck, India was directly used as a solvent and reducing agent during the preparation of Fe_3O_4 core particles. Methylene blue (MB) ($C_{16}H_{18}ClN_3S$) and methyl orange (MO) ($C_{14}H_{14}N_3NaO_3S$), procured from Matheson Coleman and Bell, USA, were used as cargo molecules for sorption studies at variable pH values. Analytical grade $FeCl_3$ was purchased from Merck Life Science Private Limited, India. *p*-Acetamido phenol (*p*-AP) (L Light Comp. Ltd, UK) and vancomycin (Incepta Pharmaceuticals Ltd, Bangladesh) were used without purification. NH_4OH (25%), HCl, anhydrous CH_3COONa, KOH and other chemicals were of reagent grade. Distilled water was further deionized by passing through an ion-exchange column, and ethanol was distilled using a Pyrex glass distillation kit.

2.2. Synthesis of mesoporous Fe_3O_4 core-particles

The magnetic core-particles were synthesized by a solvothermal process with minor revision of the procedure and recipe.[41] Briefly, 2.70 g of $FeCl_3$ and 7.20 g of anhydrous CH_3COONa were dissolved in 80.0 g of ethylene glycol. The homogenous yellow solution was put into a Teflon-lined stainless-steel autoclave and heated to 180 °C in an oven for 8 h. The autoclave was taken out and cooled to room temperature. The obtained black-colored suspension of magnetite particles was repeatedly washed *via* magnetic separation and decantation using ethanol, and finally dried under vacuum.

2.3. Synthesis of mesoporous Fe_3O_4/SiO_2 composite seed particles

The Fe_3O_4/SiO_2 composite seed particles were synthesized using a sol–gel technique.[41] Initially, 2.0 g of Fe_3O_4 core-particles and 0.02 g of CTAB powder were dispersed in 20.0 mL of ethanol using an ultrasonic vibrator for 3 min. The resultant mixture was transferred to a three-necked round flask and stirred vigorously, maintaining a nitrogen atmosphere. Subsequently, excess ethanol (135.0 mL), CTAB powder (0.80 g), and 25% ammonia solution (60.0 g) were introduced into the reaction flask. The reaction flask was heated to 70 °C, 3.0 g of TEOS was added, and the hydrolysis reaction was allowed to proceed for 8 h. The ultimate product was recovered magnetically and washed several times with distilled water. The cleaned Fe_3O_4/SiO_2 composite particles collected in acetone were finally refluxed for 24 h at 65 °C to drive off CTAB trapped within the pores. The refluxed composite seed particles were recovered magnetically and washed with deionized water in order to eliminate any remaining non-magnetic components.

2.4. Incorporation of vinyl functionality on the Fe_3O_4/SiO_2 composite seed particles

The Fe_3O_4/SiO_2 composite seed particles were modified with reactive C=C bonds using the MPS coupling agent. 1.20 g of Fe_3O_4/SiO_2 composite particles and 1.80 g of MPS were dispersed in 100 mL of a water–ethanol mixture containing 12.5 vol% water. The suspension was taken in a three-necked round flask, and mechanically stirred at 400 rpm for 24 h at 25 °C in an inert nitrogen atmosphere. The functionalized Fe_3O_4/SiO_2 composite particles were isolated by applying a magnetic field, and then subjected to multiple rounds of washing with ethanol and water. Finally, the functional composite particles were collected in distilled water.

2.5. Preparation of Fe_3O_4/SiO_2/P(2-CEA) composite polymer particles

Fe_3O_4/SiO_2/P(2-CEA) composite polymer particles were synthesized by seeded emulsion polymerization. Initially, 40 g of vinyl functionalized Fe_3O_4/SiO_2 composite seed emulsion (solid content, 0.95 g) and 0.76 g of 2-CEA were taken in a three-necked round glass reactor suspended in a thermostat hot water bath and heated to 70 °C. After 30 min of equilibration, anionic KPS (0.0304 g) aqueous initiator solution was introduced to start polymerization. The reaction mixture was agitated at 90 rpm for 24 h in an inert nitrogen atmosphere. The brownish suspension was washed several times with distilled water, and lastly collected in distilled water.

2.6. Characterizations

The change in surface functionality following chemical modification of Fe_3O_4 core particles was assessed using Fourier Transform IR (FTIR) spectroscopy (PerkinElmer, FTIR-100, USA). The sample preparation was conducted in KBr pellets. The elemental composition of the surface was assessed using an X-ray photoelectron spectrometer, XPS (PHI X-tool, ULVAC-PHI, Inc. Japan) fitted with monochromatic Al Kα radiation (1486.6 eV) operated at 50 W and 15 kV with an X-ray current of 20 μA. The XPS sample was washed, dried, and fixed on an indium plate before recording the spectra. The pressure in the measuring chamber was maintained at around 8.0×10^{-7} Pa. The survey spectra were obtained with a step size of 0.25 eV and a pass energy of 280.0 eV. A scanning electron microscope (SEM) (JSM-6510, JEOL, Tokyo, Japan) was used for understanding the surface morphology and size distribution of the prepared core particles and corresponding composites. The specimens were

diluted and deposited onto a mica substrate, where they were desiccated under vacuum conditions. Prior to SEM observation at a voltage of 20 kV, a layer of gold was deposited onto the dried samples to prevent sample damage. A transmission electron microscope (TEM) (JEM-1230, JEOL, Japan) controlled at a voltage of 100 kV was also used to understand the internal morphology. The pore volume and average pore diameter were determined by the Barrett–Joyner–Halenda (BJH) method, and the specific surface area (S_{BET}) was measured by the Brunauer–Emmett–Teller (BET) method using the NOVA3000e (Japan) surface area and pore size analyzer. The average hydrodynamic diameters of the composite polymer particles were measured by dynamic laser scattering (DLS) technique using the NICOMP 380 Particle Sizer (Santa Barbara, California, USA) at various pH levels. Each set of measurement was repeated two times and the mean value was reported. For such measurement, the dispersion was diluted with distilled water until the solid content reached approximately 0.01%. The pH-dependent change in the zeta potential was measured by a zeta potential-coupled particle size analyzer (Zetasizer Nano, Malvern Instruments Limited, UK). The powder samples were subjected to X-ray diffraction (XRD) investigation utilizing a scanning X-ray diffractometer (Bruker D8 Advance, Germany) that used Cu Kα radiation (λ = 1.5406 Å) as its source. The XRD measurements were performed using a tube voltage of 33 kV and a tube current of 45 mA. Intensity measurements were recorded at 2θ values spanning from 10° to 80°, using a constant scanning rate of 1° min^{-1}. Afterwards, the obtained spectra were processed using semi-quantitative phase analysis software to remove noise, enhance the data, and detect peaks. The thermal stability of the dried samples was studied using a thermogravimetry analyzer (TGA) (Seiko Instrument Inc. EXSTAR-6000, Japan). The samples (~10–12 mg) were heated at a rate of 30 °C min^{-1} under a flowing nitrogen environment from 30 to 800 °C, and the mass loss (%) was noted. The magnetic property was analyzed using a vibrating sample magnetometer (VSM) from Micro Sense (model EV9, USA). The pH was measured by a pH meter (Mettler-Toledo GmbH, UK). The sample was dried in an electric oven (Taisite FCO-30D, New York, USA).

2.7. Sorption of dye from aqueous solution

The sorption of MB and MO on synthesized Fe_3O_4/SiO_2/P(2-CEA) composite polymer particles was carried out in a batch process from their aqueous solutions. For the measurements, 50 mL of dye aqueous solution (0.02 mg mL^{-1}) and 10 mg of Fe_3O_4/SiO_2/P(2-CEA) composite polymer particles were mixed. The pH value was then adjusted to pH 4.0 by dropping 0.1 N HCl. Finally, the mixture was mechanically stirred at 150 rpm for specified time intervals. At the interval of 1 min, an aliquot of the sample was collected and particles were isolated using an external magnet. The residual dye concentration in the supernatant was measured by a UV-Visible spectrophotometer (UV-1280, Shimadzu, Japan) at wavelengths of 662 nm (for MB) and 465 nm (for MO). The amount of dye sorbed (q_e) by the Fe_3O_4/SiO_2/P(2-CEA) composite polymer particles was calculated using the following equation:

$$q_e = \frac{(C_0 - C_e)}{W} \times V \quad (1)$$

Here, q_e is the amount of dye sorption in mg g^{-1} of composite particles, C_0 is the initial dye concentration (mg mL^{-1}) prior to sorption, and C_e is the concentration (mg mL^{-1}) of the dye in the supernatant. It should be noted that the calibration curves (Fig. S1 and S2†) were constructed at different pH values to obtain the excess dye concentration in the supernatant.

The identical procedure was repeated at pH 10.0 for the sorption of MB and MO.

2.8. *In vitro* loading and release of bioactive molecules

The bioactive molecules, vancomycin and *p*-AP, were used as model drugs for understanding the *in vitro* loading and release behavior. The drug loading was carried out at pH 4.0, and the release was separately carried out at pH 8.0 and 10.0. The procedure is outlined below.

The pH value of a 12.5 mL aqueous suspension containing 50.0 mg of Fe_3O_4/SiO_2/P(2-CEA) composite polymer particles was adjusted to 8.1 (isoelectric point of vancomycin). Then, 10.0 mg of vancomycin, *i.e.*, 200.0 mg g^{-1} of the composite polymer was solubilized in the suspension. The mixture was kept for 35 min at 25 °C with occasional shaking. After 35 min, the pH value was adjusted to 4.0 using dil. HCl and kept for 25 min at 25 °C. After that, the composite polymer particles were magnetically recovered. The biomolecule concentration in the supernatant was determined by a UV-visible spectrophotometer at the wavelength of 280 nm. The amount of encapsulated drug molecules was calculated by subtracting the excess vancomycin in the supernatant from the initial amount. For this purpose, a calibration curve (Fig. S3a†) was used. It was assumed that at the isoelectric pH 8.1,[52] vancomycin is neutral and the P(2-CEA) polymer valve is opened due to the partial deprotonation of the carboxyl groups. So, the absence of ionic repulsion at pH 8.1 between vancomycin and the composite particles should favor its loading through the porous channel. After loading, the polymer gate valve was subsequently closed upon reduction of the pH to 4.0, blocking the leakage or release of encapsulated vancomycin. The time-dependent release behavior was monitored by re-dispersing the vancomycin-loaded Fe_3O_4/SiO_2/P(2-CEA) composite polymer particles in fresh phosphate buffer solution (PBS) at pH 10.0. The drug release was monitored at 25 °C until a steady value was reached. In order to understand the effect of pH on the release behavior, a similar release experiment was performed at pH 8.0. Calibration curves used for estimating the time-dependent release are shown in Fig. S3b and c.†

Identical loading and release experiments of *p*-AP on the Fe_3O_4/SiO_2/P(2-CEA) composite polymer particles were carried out using a slightly changed procedure. For *p*-AP loading, 50.0 mg of Fe_3O_4/SiO_2/P(2-CEA) of the composite polymer particles were dispersed in 12.5 mL of distilled water. An aqueous solution of *p*-AP (0.1875 mg, *i.e.*, 6.0 mg g^{-1} of composite polymer) was added, and the pH value was adjusted to 8.1 using dil. NaOH. The mixture was allowed to equilibrate for 35 min with occasional shaking at 25 °C. It should be noted

that *p*-AP is negatively charged at pH values above 9.5.[53] After that, the pH value of the Fe_3O_4/SiO_2/P(2-CEA) composite – *p*-AP mixture was reduced to 4.0, and then allowed to equilibrate for another 25 min to encase the loaded drug molecules inside the void space. Lastly, the *p*-AP loaded composite polymer particles were magnetically recovered. The amount of *p*-AP loading and subsequent time-dependent release were measured at the wavelength of 243 nm by following the same procedure as discussed above for vancomycin. The calibration curves used for the purpose are shown in Fig. S4.†

2.9. Hemocompatibility study

The hemolytic behavior of composite particles was studied according to a slightly modified method, as reported elsewhere.[28] Fresh human blood (10.0 mL), collected from a healthy donor (first author), was immediately centrifuged at 2500 rpm for 5 min. The residual red blood cells (RBCs) were repeatedly (3 times) washed with saline water (0.9% NaCl), and finally collected in saline. The washed RBC suspension (10 mL) was then mixed with variable concentrations (0.6, 0.7 and 0.8 mg mL^{-1}) of the respective Fe_3O_4/SiO_2 composite seed and composite polymer particles. The pH of the respective suspension was then adjusted to 7.4. TritonX-100 (1% aqueous solution) and physiological saline (0.9% NaCl) were used as the positive and negative control, respectively. All samples were incubated for 1 h at 37 °C with gentle intermittent shaking (20 min interval). After incubation, both RBCs and magnetic composite particles were separated by centrifugation (2500 rpm, 5 min). The supernatant solutions were again incubated for 30 min at 25 °C to oxidize the hemoglobin. Time-dependent (60, 90 and 120 min) hemolytic activities were also measured in the presence of 0.6 mg mL^{-1} of either composite seed or polymer particles. The absorbance of each supernatant was measured at 540 nm, and the corresponding hemolysis percent (*H*%) was calculated by applying the following equation:

$$\%\ \text{hemolysis} = \frac{\text{Abs}_{\text{sample}} - \text{Abs}_{\text{negative control}}}{\text{Abs}_{\text{positive control}} - \text{Abs}_{\text{negative control}}} \times 100$$

3. Results and discussion

3.1. Characterization

FTIR spectra were recorded to confirm the formation of Fe_3O_4 particles and the step-wise modifications carried out for the preparation of the Fe_3O_4/SiO_2/P(2-CEA) composite polymer particles.[25] Fig. 1 displays the FTIR spectra of the Fe_3O_4 core-particles, Fe_3O_4/SiO_2 composite seed and Fe_3O_4/SiO_2/P(2-CEA) composite polymer particles. The intense broad band appearing at 3401 cm^{-1} in the spectrum of the Fe_3O_4 core-particles (Fig. 1a) corresponds to the stretching vibration of the O–H bonds of the hydroxyl groups derived from absorbed water or moisture. The Fe–O stretching vibrations appear at frequencies of 445, 626 and 1618 cm^{-1}.[25,54] The bands at 2851 and 2920 cm^{-1} correspond to the stretching vibrations of the C–H groups, which originated from the adsorbed/absorbed ethylene glycol and residual templating agent CTAB.[41] The spectral analysis of the Fe_3O_4/SiO_2 composite seed particles (Fig. 1b) was conducted following a 24 h reflux in acetone at a temperature of 65 °C. The absorption signals at 1100 and 790 cm^{-1} are assignable to the vibrational modes of the Si–OH and Si–O–Si groups.[9,55] The strong dual signals detected within the 2858–3000 cm^{-1} range are indicative of the aliphatic C–H stretching vibrations originated from the ethyl groups of TEOS. The presence of these bands substantiates the creation of SiO_2 on the surface of the magnetite core-particles. In contrast, the spectrum of the Fe_3O_4/SiO_2/P(2-CEA) composite polymer particles shown in Fig. 1c exhibits a suppression in the intensity of the typical signals from the SiO_2 layer. In addition, there is a distinct peak at 1725 cm^{-1} which corresponds to the specific stretching of the C=O bonds derived from each ester and carboxyl groups of the P(2-CEA) layer.[9] From the results above, it can be said that the 2-CEA polymer is grafted onto the mesoporous Fe_3O_4/SiO_2 composite seed particles.

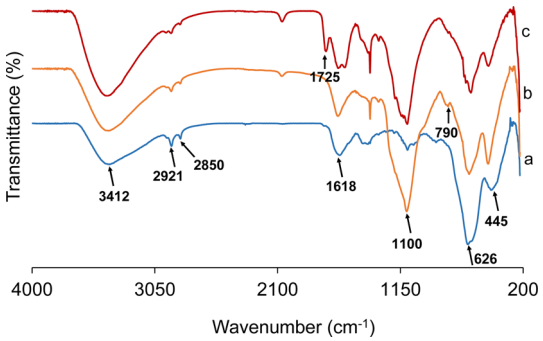

Fig. 1 FT-IR spectra of (a) Fe_3O_4 core-particles, (b) Fe_3O_4/SiO_2 composite seed particles and (c) Fe_3O_4/SiO_2/P(2-CEA) composite polymer particles.

The surface elemental compositions were verified by XPS, as depicted in Fig. 2. The survey spectrum of the Fe_3O_4 core-particles (Fig. 2a) shows the presence of the Fe2p signal at 710.5 eV. The Fe2p signal is distinguishable into two distinct doublets attributable to the $Fe2p_{3/2}$ and $Fe2p_{1/2}$ core-level signals of ferric oxides.[41,56] The spectrum of the Fe_3O_4/SiO_2

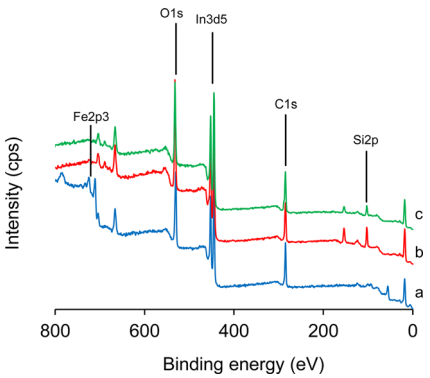

Fig. 2 XPS spectra of (a) Fe_3O_4 core-particles, (b) Fe_3O_4/SiO_2 composite seed particles, and (c) Fe_3O_4/SiO_2/P(2-CEA) composite polymer particles.

composite seed particles (Fig. 1b) exhibits a distinct Si2p signal in the 102–150 eV region. Following the surface coverage by the SiO_2 layer, the overall intensity of the Fe2p signal is reduced to 1.92 at% from the initial 15.44 at% in the Fe_3O_4 core-particles. However, in the survey spectrum of the Fe_3O_4/SiO_2/P(2-CEA) composite polymer particles (Fig. 1c), the Si2p signal strength is only scarcely reduced from 7.66 at% to 7.31 at% after the seeded emulsion polymerization. These findings indicate that the Fe_3O_4/SiO_2 composite seed particles do not have complete coverage by the pH-sensitive P(2-CEA), and the polymerization might have occurred mostly within and around the mesopore structure. As a result, the mesoporous surface structure of the Fe_3O_4/SiO_2/P(2-CEA) composite polymer particles is possibly maintained. Obviously, the C1s signal intensity considerably increases from 38 at% in the Fe_3O_4/SiO_2 composite seed particles to 45 at% in the Fe_3O_4/SiO_2/P(2-CEA) composite polymer particles.

Fig. 3 shows the XRD patterns of the Fe_3O_4 core-particles, Fe_3O_4/SiO_2 composite seed particles, and Fe_3O_4/SiO_2/P(2-CEA) composite polymer particles. The presence of sharp peaks at 2θ values of 30.10°, 35.42°, 43.05°, 53.39°, 56.94° and 62.52° in the XRD pattern of Fe_3O_4 particles (Fig. 1a) indicates that iron oxide possesses a crystalline cubic spinal structure, as discussed in the report of JCPDS-International Centre (JCPDS file no. 19-0629).[57] The broad band averaged at about 20° in Fig. 1b is due to the amorphous SiO_2 coverage on the Fe_3O_4 particles. Comparatively, in the diffraction pattern of the Fe_3O_4/SiO_2/P(2-CEA) composite polymer particles (Fig. 1c), the broad amorphous reflection became relatively flat, suggesting that a change in the surface composition and polymerization probably occurred inside the pore, as also predicted from XPS spectral analysis. The average crystallite sizes of iron oxide in the Fe_3O_4 core-particles, Fe_3O_4/SiO_2 composite seed particles, and Fe_3O_4/SiO_2/P(2-CEA) composite polymer particles are around 8, 12 and 7 nm, respectively. Hence, from the overall diffraction patterns, it is conceivable that the cubic spinal structure of Fe_3O_4 is maintained in the Fe_3O_4/SiO_2/P(2-CEA) composite polymer particles during surface modification.

The surface morphology and size distribution by SEM images are illustrated in Fig. 4. The Fe_3O_4 core-particles, shown in Fig. 4a, are spherical and slightly polydispersed. The surface appears rough and heterogeneous (inset image), perhaps due to the mesoporous structure. The average diameter and coefficient of variation (CV) of the Fe_3O_4 core-particles, measured by the ImageJ software, are 414 nm and 35%, respectively. It should be noted that the solvothermal process usually demonstrates a comparatively higher polydispersity index.[41] The surface heterogeneity and spherical identity of the Fe_3O_4/SiO_2 composite seed particles (Fig. 4b) are almost retained following silica coverage. An increasing number of smaller particles, possibly SiO_2 particles, are firmly adhered to the surface of the Fe_3O_4 core-particles. The average diameter of the composite seed particles is increased to 574 nm, and the CV is 25%. It can be assumed that the Fe_3O_4/SiO_2 composite seed particles do not contain any nonmagnetic free SiO_2 particles, as the particles were repeatedly washed *via* magnetic separation and decantation. After seeded emulsion polymerization, the surface of the Fe_3O_4/SiO_2/P(2-CEA) composite polymer particles (Fig. 4c) becomes relatively smooth. The average diameter of the Fe_3O_4/SiO_2/P(2-CEA) composite polymer particles further increases to 596 nm. It is apparent from the image (Fig. 4c) that some sort of bridged flocculation might have proceeded during the sample preparation for the Fe_3O_4/SiO_2/P(2-CEA) composite polymer particles. However, on standing, the as-prepared washed composite polymer suspension remained moderately stable and dispersed up to 1 h (Fig. S5†). The particles were sedimented on prolonged standing, but the dispersion state was revived upon shaking. Such distortion of shape is also possible during observation, as the acrylate polymer is sometimes not stable under an electron beam.[58] In order to assess the mesoporous structure and internal morphology, the high-resolution TEM image of the Fe_3O_4/SiO_2/P(2-CEA) composite polymer particles was analyzed, as shown in Fig. 4d. The dense region represents the solid parts and the lighter region represents the porous structure. The average diameter and CV measured from TEM is around 596 nm and 27%, and matches well with the SEM image. The gradual increase in the average diameter and internal morphology suggests that the mesoporous Fe_3O_4/SiO_2/P(2-CEA) composite polymer particles were successfully prepared.

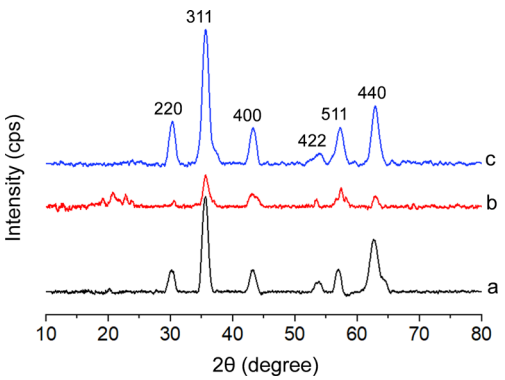

Fig. 3 XRD spectra of the (a) Fe_3O_4 core-particles, (b) Fe_3O_4/SiO_2 composite seed particles, and (c) Fe_3O_4/SiO_2/P(2-CEA) composite polymer particles.

The presence of a mesoporous structure has been verified through the use of Brunauer–Emmett–Teller (BET) surface analysis. The average BJH pore diameter in the Fe_3O_4 core-particles is 3.85 nm, confirming the mesoporous structure.[59] Following SiO_2 coverage, the average pore diameter increased to 29.73 nm, *i.e.*, the mesoporous structure in the Fe_3O_4/SiO_2 composite seed particles is still maintained. Importantly, after seeded emulsion polymerization, the mean pore diameter is decreased to 3.41 nm in the Fe_3O_4/SiO_2/P(2-CEA) composite polymer particles. Polymerization of 2-CEA in and around the pore might have reduced the pore diameter. This assumption is in conformity with our earlier prediction from the XPS (Fig. 2) and XRD (Fig. 3) results. The average specific surface area (S_{BET}) of the Fe_3O_4 core-particles, Fe_3O_4/SiO_2 composite seed particles and Fe_3O_4/SiO_2/P(2-CEA) composite polymer particles are 19.55, 7.23 and 20.29 $m^2\ g^{-1}$, respectively. The increase in the surface area for the composite polymer particles is possibly associated

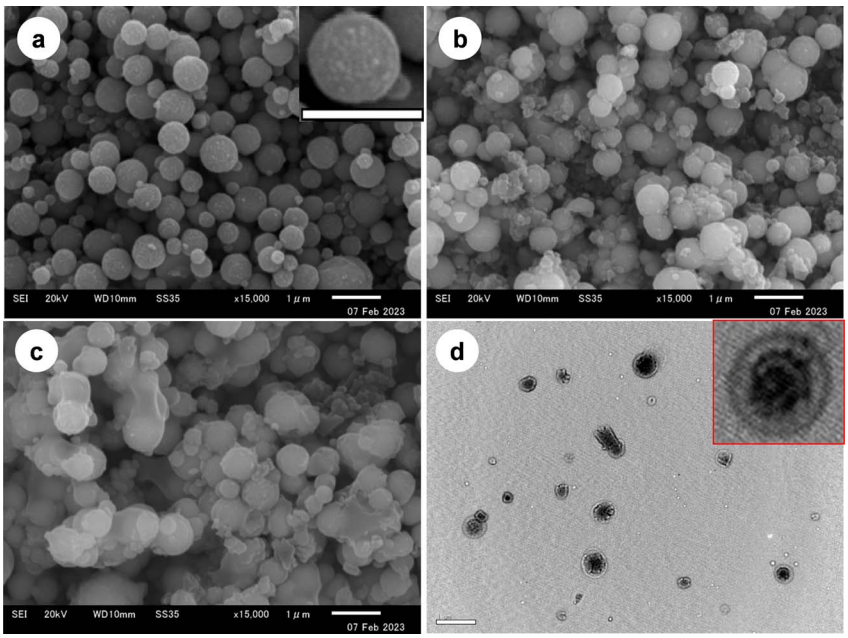

Fig. 4 (a–c) SEM and (d) high-resolution TEM images of (a) Fe_3O_4 core-particles, (b) Fe_3O_4/SiO_2 composite seed particles, and the (c and d) Fe_3O_4/SiO_2/P(2-CEA) composite polymer particles. The scale bar represents 1 μm scale.

with an improvement in the colloidal stability, following the formation of a polymer layer around the magnetic SiO_2 particles. The nitrogen adsorption–desorption isotherms of the Fe_3O_4 core-particles, Fe_3O_4/SiO_2 composite seed particles, and Fe_3O_4/SiO_2/P(2-CEA) composite polymer particles, shown in Fig. S6,† exhibit an identical type IV mesoporous structure for all materials.[9] The volume of nitrogen adsorption in the respective core and composite polymer particles is close to each other. Accordingly, they have an almost identical average specific surface area and pore diameter. Conversely, the Fe_3O_4/SiO_2 composite seed particles possess the lowest adsorption owing to the maximum average pore diameter (29.73 nm) and the minimum specific surface area (7.23 $m^2\ g^{-1}$). The open hysteresis for the Fe_3O_4 core-particles and Fe_3O_4/SiO_2/P(2-CEA) composite polymer particles with desorption isotherms lying above the adsorption isotherms are possibly attributed to the mesoporous structures with nanopores that possibly slowed down the adsorption kinetics.[60,61] This open hysteresis phenomenon in the Fe_3O_4/SiO_2/P(2-CEA) composite polymer particles can also arise from the swelling effect of the organic P(2-CEA) polymer.

The thermal stability and inorganic content were measured by studying the thermal decomposition of the Fe_3O_4 core-particles, Fe_3O_4/SiO_2 composite seed particles and Fe_3O_4/SiO_2/P(2-CEA) composite polymer particles, as shown in Fig. 5. The TG curve of the Fe_3O_4 core-particles (Fig. 5a) shows two separate mass loss regions. The initial mass reduction up to 150 °C corresponds to the volatilization of ethanol and moisture, absorbed during particle washing. The second notable mass reduction in the temperature range of 215–292 °C is resulted from the decomposition of trapped ethylene glycol.[28] The second mass loss in the Fe_3O_4/SiO_2 composite seed particles (Fig. 5b) is started at a somewhat higher temperature (250 °C). In this case, the mass loss refers to the elimination of the organic part of TEOS and any remaining CTAB that is trapped within the mesoporous structure.[28,41] On the contrary, the Fe_3O_4/SiO_2/P(2-CEA) composite particles (Fig. 5c) exhibit a distinct and sharp reduction in mass in the temperature range of 187–468 °C. A relative study shows that the Fe_3O_4/SiO_2/P(2-CEA) composite particles contained approximately 27% organic P(2-CEA).

The magnetic characteristics of the dehydrated powder samples of the Fe_3O_4 core-particles, Fe_3O_4/SiO_2, and Fe_3O_4/SiO_2/P(2-CEA) composite particles were examined using VSM, and a comparative plot of the hysteresis loops is depicted in Fig. 6. The magnetic hysteresis curve of the Fe_3O_4 core-particles (Fig. 6a) reveal the saturation magnetization (M_s) as around 52.80 emu g^{-1}. The magnetization curve's reversible nature and

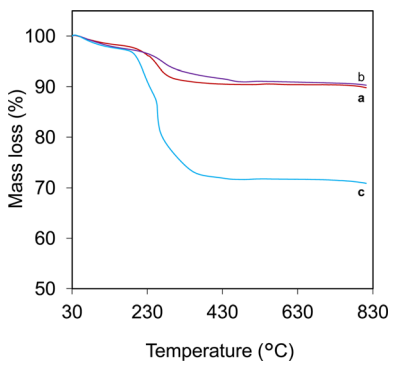

Fig. 5 TGA spectra of (a) Fe_3O_4 core-particles, (b) Fe_3O_4/SiO_2 composite seed particles, and (c) Fe_3O_4/SiO_2/P(2-CEA) composite polymer particles.

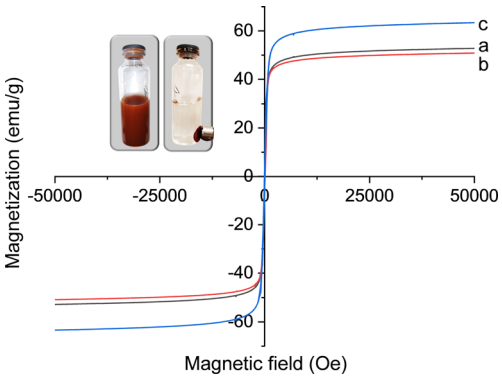

Fig. 6 The hysteresis loops of (a) Fe_3O_4 core-particles, (b) Fe_3O_4/SiO_2 composite seed particles, and (c) Fe_3O_4/SiO_2/P(2-CEA) composite polymer particles. Inset: magnetic separation of Fe_3O_4/SiO_2/P(2-CEA) composite polymer particles.

the almost-zero coercivity (H_c) indicate a paramagnetic characteristic. The M_s value of the Fe_3O_4/SiO_2 composite particle (Fig. 6b) is decreased to 50.88 emu g^{-1}, which is caused by the inclusion of nonmagnetic SiO_2.[62] In contrast, the value of M_s of the Fe_3O_4/SiO_2/P(2-CEA) composite polymer particles (Fig. 6c) noticeably improved to 63.42 emu g^{-1}. In general, the formation of a nonmagnetic layer on the magnetic particles reduces the M_s.[25] The unexpected increase in the M_s value of the composite polymer particles is possibly related to the improvement in the crystal structure and stability to surface oxidation.[63,64] In addition to this, the improvement in stability following polymer coating should decrease the disorder of the spins on the surface and consequently, the magnetization is enhanced.[63] The almost classic "S"-shaped reversible magnetization curve of the Fe_3O_4 core-particles was preserved during chemical modification. It is also evident (inset figure) that composite polymer particles can be effectively isolated from the dispersion medium by an external magnet, leaving an apparently clear supernatant.

3.2. pH-dependent phase transition of the composite polymer particles

Fig. 7a illustrates the pH-dependent variations in the average hydrodynamic diameter of the Fe_3O_4/SiO_2/P(2-CEA) composite polymer particles. The average hydrodynamic diameter exhibits a progressive reduction as the pH increases from 2 to 10. At lower pH value, the surface of the composite particles should be hydrophobic because the carboxyl groups of the P(2-CEA) segments are in the protonated (–COOH) state. Hence, polymers are supposed to be all collapsed on the particles surface. However, Fig. 7a demonstrates the opposite result, *i.e.*, the hydrodynamic diameter increased in the acidic pH region. It is likely that the nonionic nature and paramagnetic property of the Fe_3O_4/SiO_2/P(2-CEA) composite polymer particles promoted the partial aggregation of particles. This also produced sedimentation of the composite polymer particles within 10 min, as shown in the inset of Fig. 7a. Whereas, in the alkaline range (pH > 7), the carboxyl groups are deprotonated ($–COO^-$) increasingly more with the increase of the pH value. The ionization of the carboxyl groups resulted in repulsion among the polymer chains lying in and around the mesoporous channels, and the opening of the gate valve. The opening of the anionic polymer gate valve, which functioned as a hairy structure, favored repulsion among like-charged magnetic composite polymer particles, and ultimately stabilized the suspension. This improved stability might have contributed to the reduction in the hydrodynamic diameter at the higher pH region. The digital image shown in the inset of Fig. 7a also confirmed the improvement in stability with increasing pH value.

The pH-dependent changes in the zeta potential shown in Fig. 7b further confirms the protonation and deprotonation of the composite polymer particles. Undoubtedly, as the pH of the diluted composite suspension increases from 2 to 10, the zeta potential values exhibit a gradual increase in negativity due to the ionization of the carboxyl groups of P(2-CEA). Hence, the composite polymer particles became kinetically and electrostatically stable in the higher pH region.

3.3. Sorption of methylene blue (MB) and methyl orange (MO) dyes

The time-dependent sorption behavior of cationic MB and anionic MO was investigated on the Fe_3O_4/SiO_2/P(2-CEA) composite polymer particles at pH values of 4.0 and 10.0, respectively. This sorption experiment was carried out to confirm the variation in the surface property of composite polymer particles with changing pH values. In the following section, the term 'sorption' is used as the composite polymer particles are mesoporous in nature. Fig. 8a shows that the amount of sorption of cationic MB is lower at pH 4.0 than that at

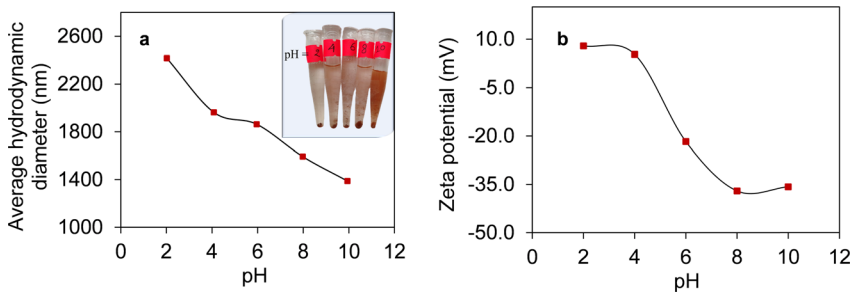

Fig. 7 pH-dependent changes in the (a) average hydrodynamic diameter and (b) zeta potential of Fe_3O_4/SiO_2/P(2-CEA) composite polymer particles. Inset in (a): pH-dependent stability of Fe_3O_4/SiO_2/P(2-CEA) composite polymer particles.

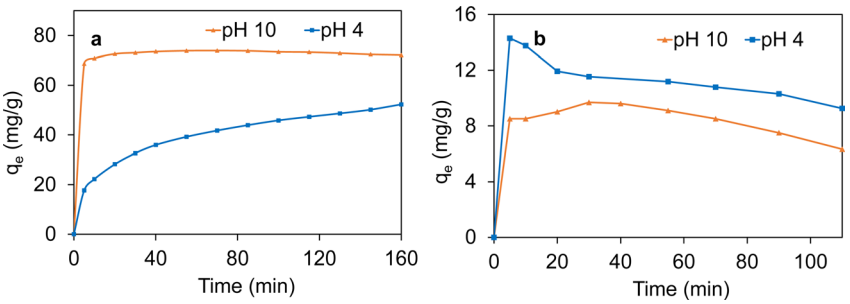

Fig. 8 Sorption behavior of (a) cationic MB and (b) anionic MO dye molecules on Fe_3O_4/SiO_2/P(2-CEA) composite polymer particles. Conditions: temperature, 25 °C; dye, 0.02 mg mL^{-1}; composite polymer particles, 10 mg; and total volume, 50 mL.

pH 10.0. It is obvious that the composite polymer particles are negatively charged at pH 10.0 due to deprotonation of the carboxyl groups of the P(2-CEA) unit. This increases the amount of sorption of cationic MB on the anionic Fe_3O_4/SiO_2/P(2-CEA) composite polymer particles through electrostatic attraction. The electrostatic attraction also accelerated the sorption process and nearly reached almost saturation within 5 min. Whereas, at pH 4.0, such attractive force is absent as the composite polymer particles become neutral. The sorption at pH 4.0 is therefore attributed to only hydrophobic interactions between the composite polymer particles and cationic MB. In contrast, the anionic MO shows the opposite sorption behavior, as illustrated in Fig. 8b. The amount of sorption at pH 10.0 of the anionic MO is expectedly lower than that at pH 4.0. The electrostatic repulsion between the negatively charged particles and anionic MO reduces the amount of sorption at pH 10.0. A comparative sorption behavior shows that the sorption amount of MO is slightly decreased after reaching the maximum value. Mechanical stress from intermittent shaking possibly results in a partial release of the surface-adsorbed MO with increased time, as this dye molecule has relatively lower molecular weight and is also comparatively less hydrophobic. Nonetheless, the above sorption behavior of the cationic MB and anionic MO confirms the pH-responsive surface properties of the Fe_3O_4/SiO_2/P(2-CEA) composite polymer particles.

3.4. Loading and release behavior of active molecules

Mesoporous magnetic pH-responsive Fe_3O_4/SiO_2/P(2-CEA) composite polymer particles can be useful for the controlled delivery of active drug molecules. Mesoporous magnetic silica particles with 2-CEA polymer on the surface are of great interest because the structure of P(2-CEA) in aqueous solution is pH-dependent. At higher pH (pH $\geq$ 8), almost all carboxyl groups are deprotonated in aqueous solution and the 2-CEA polymer chains are highly swellable due to the ionic repulsion that open the mesoporous channels for drug loading (Fig. S7†). On the other hand, at pH $\leq$ 4, the swelling ability of the P(2-CEA) chains decreases due to protonation of the carboxyl groups. Thus, the polymer chains collapse around the mesoporous channels and block the pores. The polymer chain can thus act as a valve that can regulate the encapsulation and release of drug molecules loaded inside the porous channels.

In order to prove the pH-stimuli regulated loading and release of drug molecules from the Fe_3O_4/SiO_2/P(2-CEA) composite polymer particles, vancomycin and *p*-AP have been selected as two model drugs. The drug loading pH conditions were carefully chosen to ensure the neutrality of the drug molecules during loading and swelling, *i.e.*, opening of the 2-CEA polymer gate valve, followed by deswelling, *i.e.*, closing of the gate valve. Fig. 9a shows the amount of vancomycin encapsulated at pH 4.0, and their subsequent gradual release at pH 8.0 and 10.0 with time. A considerable amount of vancomycin (106.19 mg g^{-1} of composite) is loaded at pH 4.0 inside the mesoporous channel of the composite polymer particles. This loaded vancomycin is equivalent to approximately 5.3 mg of added 10 mg during the loading experiment. Hence, the loading efficiency is around 53%. The gradual release observed for vancomycin at pH 10.0 from the drug-loaded Fe_3O_4/SiO_2/P(2-CEA) composite polymer particles in fresh PBS is fairly rapid. About 94% of loaded vancomycin is released within 45 min, and nearly all (99%) encapsulated drug molecules are released after 165 min. Comparatively, the release is slow at pH 8.0, but still reached 87% after 225 min, which is satisfactory for drug delivery application. The pH-dependent uptake and release of *p*-AP shown in Fig. 9b demonstrates that the amount of loading in the Fe_3O_4/SiO_2/P(2-CEA) composite polymer particles is 5.0 mg g^{-1} of the composite particles at pH 4.0. Hence, about 83% of the added drug (6.0 mg g^{-1}) is loaded in the composite polymer particles. Relative to vancomycin (1449.3 g mol^{-1}), the molecular weight of *p*-AP (151.163 g mol^{-1}) is low and is more hydrophobic. This property may have enhanced the loading and encapsulation of *p*-AP at pH 4.0. The drug release at pH 10.0 is fairly rapid again, releasing around 40% of the loaded drug molecules within 45 min. With increasing time, the release increased to around 46% after 225 min. At pH 8.0, the release of *p*-AP is comparatively low, but still reached 37% after 225 min. As a direct proof of the above results, the drug release profiles of vancomycin and *p*-AP are illustrated in Fig. S8.† In each case, the increase in the absorption maximum with the release time suggests that the amount of release increases. Therefore, the above experiments confirmed that the mesoporous magnetic Fe_3O_4/SiO_2/P(2-CEA) composite polymer particles can be applied as a pH-stimuli responsive drug carrier for targeted drug release to specific locations where the pH is favorably alkaline.

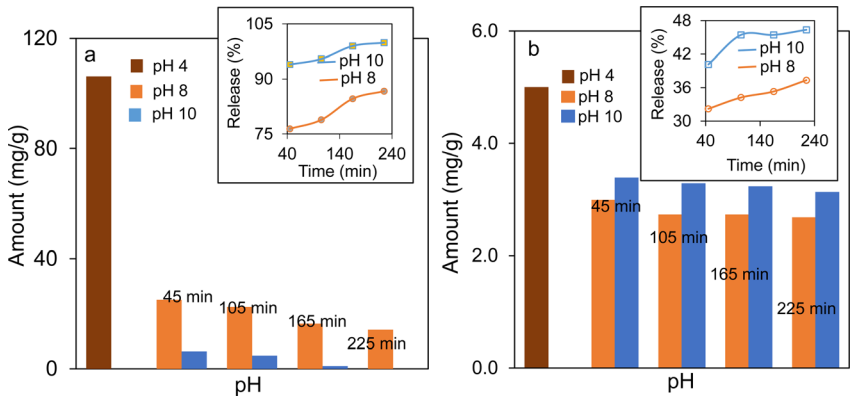

Fig. 9 Encapsulation at pH 4.0 and subsequent time-dependent release at pH 8.0 and 10.0 of (a) vancomycin and (b) *p*-AP from the Fe_3O_4/SiO_2/P(2-CEA) composite polymer particles. Inset shows the percentage of release against time.

In order to clarify the loading of the drug in the composite polymer particles at pH 4.0, a comparative plot of the FTIR spectra of vancomycin, Fe_3O_4/SiO_2/P(2-CEA) composite polymer particles and vancomycin-loaded composite polymer is evaluated as an example. The characteristic absorption signals of vancomycin (Fig. S9a†) belonging to the C=O stretching of the amide I band, C=C of the aromatic ring, and phenolic –OH groups appear at 1652, 1502 and 1230 cm^{-1}, respectively.[65] The spectrum of the vancomycin-loaded Fe_3O_4/SiO_2/P(2-CEA) composite polymer particles (Fig. S9c†) matches well with both vancomycin (Fig. S9a†) and the unloaded composite polymer particles (Fig. S9b†). The weak absorption signal of vancomycin in the drug-loaded composite polymer particles is expected as most drug molecules are localized within the porous channel and covered with the P(2-CEA) gate valve.

3.5. Hemolysis study

The hemocompatibility test is of great significance for biomaterials to determine blood compatibility. The hemolytic behavior in the presence of different amounts of the respective Fe_3O_4/SiO_2 composite seed and Fe_3O_4/SiO_2/P(2-CEA) composite polymer particles is shown in Fig. 10A. Independent of the composite particle nature, the hemolysis (%) increased with the increase in the particle concentration. The composite polymer particles at 0.7 mg mL^{-1} of the particle concentration exhibited 4.9% hemolysis, below the <5% permissible lime.[66] It is also observed that the hemocompatibility of the composite polymer particles is slightly inferior to that of the Fe_3O_4/SiO_2 composite seed particles. The presence of the hydrophobic ethyl acrylate moiety and partial ionization of the carboxyl groups at pH 7.4 are possibly accounted for the reduced hemocompatibility of the Fe_3O_4/SiO_2/P(2-CEA) composite polymer particles. Whatever the findings, it is evident that the prepared composite polymer particles are hemocompatible up to 0.7 mg mL^{-1}.

The time-dependent hemolysis percentages in the presence of the Fe_3O_4/SiO_2/P(2-CEA) composite polymer particles at a particle concentration of 0.6 mg mL^{-1} (Fig. 10B) indicated that the hemolysis degree initially increased, and then became almost steady beyond 90 min. Despite the increase, the hemolysis degree remained below the permissible limit of 5% after 120 min. The Fe_3O_4/SiO_2 composite seed particles followed the same hemolysis pattern, but the hemocompatibility is slightly higher.

The digital photographs of the supernatants of RBCs after incubation with saline water (negative control), composite seed

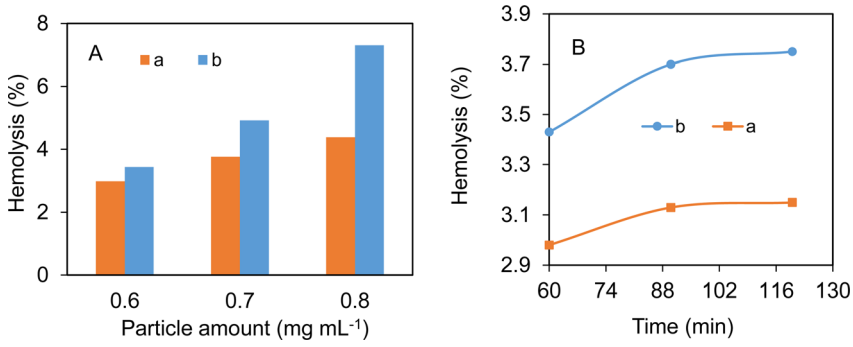

Fig. 10 (A) Hemolysis percentages in the presence of different concentrations of (a) Fe_3O_4/SiO_2 composite seed particles and (b) Fe_3O_4/SiO_2/P(2-CEA) composite polymer particles. Conditions: pH, 7.4; temperature, 37 °C; and incubation time, 1 h. (B) Change in hemolysis percentage with incubation time for (a) Fe_3O_4/SiO_2 composite seed particles and (b) Fe_3O_4/SiO_2/P(2-CEA) composite polymer particles. Conditions: particles, 0.6 mg mL^{-1}; pH, 7.4 and temperature, 37 °C.

particles, composite polymer particles and Triton X-100 (positive control) are also evaluated and displayed in Fig. S10.† The colors of the supernatants from the negative control experiment, Fe_3O_4/SiO_2 composite seed and Fe_3O_4/SiO_2/P(2-CEA) composite polymer particles are very light and nearly transparent, indicating the presence of either a negligible amount or no oxyhemoglobin. On the other hand, in the positive control experiment, the color is red due to the formation of the red colored oxyhemoglobin following interaction of RBCs with non-ionic Triton X-100.[28] Although the hemocompatibility of the Fe_3O_4/SiO_2/P(2-CEA) composite polymer particles decreased with increasing concentration, they are still hemocompatible at lower concentrations, *i.e.*, 0.6–0.7 mg mL^{-1} (estimated from the bar diagram) and can be used for intravenous applications.

4. Conclusions

This investigation is aimed at preparing pH-responsive mesoporous magnetic Fe_3O_4/SiO_2/P(2-CEA) composite polymer particles for drug delivery to specific locations of comparatively alkaline pH, such as the intestine/colon. A new least popular carboxy functional 2-CEA monomer is used for this purpose. It is believed that the presence of the P(2-CEA) polymer in and around the pore would act as a polymer valve for regulating the controlled release of toxic drug molecules loaded inside the void spaces *via* opening at the alkaline pH values. The magnetic property would help to drive the drug-loaded particles to specific locations/organs for specific times. First, sub-micrometer-sized mesoporous Fe_3O_4 core-particles are prepared by solvothermal method. The Fe_3O_4 core-particles are modified with the mesoporous SiO_2 layer to enhance the biocompatibility, as well as the drug loading capacity. To facilitate the seeded polymerization of 2-CEA from the surface, vinyl groups are introduced on the Fe_3O_4/SiO_2 composite seed particles. BET surface analysis confirmed that the Fe_3O_4/SiO_2/P(2-CEA) composite polymer particles had a mesoporous structure with an average pore diameter of 3.41 nm. The composition analysis by FTIR, XPS, and XRD suggested that the composite particles are modified with a thin layer of P(2-CEA), lying mostly within and around the pore. The crystalline cubic spinal structure of iron oxide and its average crystallite size are almost retained during the stepwise preparation. The Fe_3O_4/SiO_2/P(2-CEA) composite polymer particles displayed a high saturation magnetization value (63.42 emu g^{-1}) with a classic 'S'-shaped magnetization curve, which is typical for a strong paramagnetic property. The pH-dependent change in the hydrodynamic diameter, zeta-potential and sorption behavior of the cationic and anionic dye molecules confirmed the pH-sensitive surface property of the composite polymer. The *in vitro* loading and release experiment of two drug molecules, vancomycin and *p*-AP, showed 99% and 46.0% release at pH 10.0. Even at pH 8.0, the amount of release reached 87% and 37% for vancomycin and *p*-AP, respectively. The hemolysis study revealed that composite polymer particles are favorably hemocompatible up to a concentration of 0.7 mg mL^{-1}. Hence, it can be concluded that the Fe_3O_4/SiO_2/P(2-CEA) composite polymer particles can be used as a microcapsule for loading and the safe release of toxic drug molecules for treating intestine and colon cancer, minimizing the release and degradation of drugs while passing through the stomach.

Data availability

All the data (in figures and images) are available in the manuscript and ESI file.† No additional data are required for readers of the manuscript.

Author contributions

Most. Nusrat Jahan: methodology, investigation, formal analysis, data curation, validation, writing – original draft. Md. Ashraful Alam: funding acquisition, conceptualization. Md. Mahabur Rahman: investigation, formal analysis, data curation. S. Manjura Hoque: investigation, data curation. Hasan Ahmad: supervision, conceptualization, data curation, resources, project administration, writing – review and editing.

Conflicts of interest

There are no conflicts to declare.

Acknowledgements

The corresponding author (H. A.) gratefully acknowledges the financial grant received under special allocation from Rajshahi University for procuring instruments and chemicals in the year 2021–2022. The first author (M. N. J.) acknowledges a fellowship from the Ministry of National Science and Technology for her MSc research.

References

1 M. S. B. Reddy, D. Ponnamma, K. K. Sadasivuni, B. Kumar and A. M. Abdullah, Carbon dioxide adsorption based on porous materials, *RSC Adv.*, 2021, **11**(21), 12658–12681.
2 M. Z. Sarker, M. M. Rahman, H. Minami, T. Suzuki, M. K. Hossain and H. Ahmad, Mesoporous amine functionalized SiO_2 supported Cu nanocatalyst and a kinetic-mechanistic degradation study of azo dyes, *Colloids Surf., A*, 2021, **617**, 126403.
3 M. Rashid, M. M. Islam, H. Minami, M. Aftabuzzaman, M. A. Rahman, M. M. Hossain, S. M. Hoque, M. A. Alam and H. Ahmad, Nickel decorated melamine-formaldehyde resin/polyaniline composites for high specific capacitance, *Mater. Chem. Phys.*, 2020, **249**, 122957.
4 Y. Wu and B. M. Weckhuysen, Separation and purification of hydrocarbons with porous materials, *Angew. Chem., Int. Ed.*, 2021, **60**, 18930–18949.
5 T. T. Nguyen, N. S. N. S. Bahri, A. M. Rahmatika, K. L. A. Cao, T. Hirano and T. Ogi, Rapid indomethacin release from porous pectin particles as a colon-targeted drug delivery system, *ACS Appl. Bio Mater.*, 2023, **6**(7), 2725–2735.
6 P. Samanta, A. V. Desai, S. Let and S. K. Ghosh, Advanced porous materials for sensing, capture and detoxification of

organic pollutants towards water remediation, *ACS Sustain. Chem. Eng.*, 2019, **7**(8), 7456–7478.

7 R. Sun, S. Feng, B. Zhou, Z. Chen, D. Wang and H. Liu, Flexible cyclosiloxane-linked fluorescent porous polymers for multifunctional chemical sensors, *ACS Macro Lett.*, 2019, **9**(1), 43–48.

8 L. Kong, M. Zhong, W. Shuang, Y. Xu and X. H. Bu, Electrochemically active sites inside crystalline porous materials for energy storage and conversion, *Chem. Soc. Rev.*, 2020, **49**(8), 2378–2407.

9 M. M. Rahman, H. Minami, M. K. Hossain, M. M. Rahman, S. M. Hoque, M. R. Karim, M. S. I. Sarker and H. Ahmad, Preparation and characterization of carboxyl functional mesoporous ZnO-SiO_2 composites and in vitro sensing of glucose and vancomycin, *Sens. Actuators, B*, 2023, **393**, 134133.

10 E. Xifre-Perez, S. Guaita-Esteruelas, M. Baranowska, J. Pallares, L. Masana and L. F. Marsal, In vitro biocompatibility of surface-modified porous alumina particles for HepG2 tumor cells: toward early diagnosis and targeted treatment, *ACS Appl. Mater. Interfaces*, 2015, **7**(33), 18600–18608.

11 J. Li, K. Liu, X. Gao, B. Yao, K. Huo, Y. Cheng and L. Huang, Oxygen- and nitrogen-enriched 3D porous carbon for supercapacitors of high volumetric capacity, *ACS Appl. Mater. Interfaces*, 2015, **7**(44), 24622–24628.

12 J. Han, I. Johnson and M. Chen, 3D continuously porous graphene for energy applications, *Adv. Mater.*, 2022, **34**(15), 2108750.

13 Y. Li and J. Yu, Emerging applications of zeolites in catalysis, separation and host–guest assembly, *Nat. Rev. Mater.*, 2021, **6**(12), 1156–1174.

14 T. T. Nuguyen, Q. A. N. Thi, N. H. Le and N. H. Nguyen, Synthesis of a novel porous Ag_2O nanomaterial on ion exchange resin and its application for COD determination of high salinity water, *Sci. Rep.*, 2011, **11**, 11487.

15 S. Xiao, S. Wang, X. Wang and P. Xu, Nanoporous gold: a review and potentials in biotechnological and biomedical applications, *Nano Sel.*, 2021, **2**(8), 1437–1458.

16 Y. J. Cheng, G. F. Luo, J. Y. Zhu, X. D. Xu, X. Zeng, D. B. Cheng and F. He, Enzyme-induced and tumor-targeted drug delivery system based on multifunctional mesoporous silica nanoparticles, *ACS Appl. Mater. Interfaces*, 2015, **7**(17), 9078–9087.

17 J. Wagner, D. Göß, N. Ustyanovska, M. Xiong, D. Hauser, O. Zhuzhgova, S. Hočevar, B. Taskoparan, L. Poller, S. Datz, H. Engelke, Y. Daali, T. Bein and C. Bourquin, Mesoporous silica nanoparticles as pH-responsive carrier for the immune-activating drug Resiquimod enhance the local immune response in mice, *ACS Nano*, 2021, **15**(3), 4450–4466.

18 B. Cong, P. Li, H. Li, C. Hong and X. Qiao, A pH-responsive hollow mesoporous SiO_2 nanocarrier designed for the ultrasensitive detection of alpha-fetoprotein, *New J. Chem.*, 2023, **47**(47), 21916–21923.

19 C. Deng, Y. Liu, F. Zhou, M. Wu, Q. Zhang, D. Yi and Y. Wang, Engineering of dendritic mesoporous silica nanoparticles for efficient delivery of water-insoluble paclitaxel in cancer therapy, *J. Colloid Interface Sci.*, 2021, **593**, 424–433.

20 X. Li, C. Xie, H. Xia and Z. Wang, pH and ultrasound dual-responsive polydopamine-coated mesoporous silica nanoparticles for controlled drug delivery, *Langmuir*, 2018, **34**(34), 9974–9981.

21 H. Ahmad, Biocompatible SiO_2 in the fabrication of stimuli-responsive hybrid composites and their application potential, *J. Chem.*, 2015, **2015**, 846328.

22 A. S. Hoffman, Stimuli-responsive polymers: biomedical applications and challenges for clinical translation, *Adv. Drug Delivery Rev.*, 2013, **65**(1), 10–16.

23 J. Zhang, Y. Lin, Z. Lin, Q. Wei, J. Qian, R. Ruan, X. Jiang, L. Hou, J. Song, J. Ding and H. Yang, Stimuli-responsive nanoparticles for controlled drug delivery in synergistic cancer immunotherapy, *Adv. Sci.*, 2022, **9**(5), 2103444.

24 Z. Xiang, M. Liu and J. Song, Stimuli-responsive polymeric nanosystems for controlled drug delivery, *Appl. Sci.*, 2021, **11**(20), 9541.

25 M. K. Hossain, H. Minami, S. M. Hoque, M. M. Rahman, M. K. Sharafat, M. F. Begum, M. E. Islam and H. Ahmad, Mesoporous electromagnetic composite particles: Electric current responsive release of biologically active molecules and antibacterial properties, *Colloids Surf., B*, 2019, **181**, 85–93.

26 Y. Nahar, M. A. Rahman, M. K. Hossain, M. K. Sharafat, M. R. Karim, A. Elaissari, B. Ochiai, H. Ahmad and M. A. Rahman, A facile one-pot synthesis of poly(acrylic acid)-functionalized magnetic iron oxide nanoparticles for suppressing reactive oxygen species generation and adsorption of biocatalyst, *Mater. Res. Express*, 2020, **7**, 016102.

27 Y. Mu, L. Gong, T. Peng, J. Yao and Z. Lin, Advances in pH-responsive drug delivery systems, *OpenNano*, 2021, **5**, 100031.

28 K. A. Bithi, H. Minami, M. K. Hossain, M. M. Rahman, M. A. Rahman, M. A. Gafur and H. Ahmad, Cationic polyelectrolyte grafted mesoporous magnetic silica composite particles for targeted drug delivery and thrombolysis, *Materialia*, 2020, **11**, 100676.

29 M. M. Rahman, Y. Nahar, M. W. U. Oli, A. Elaissari and H. Ahmad, Incorporation of iron oxide nanoparticles into temperature-responsive poly(N-isorpropylacrylamide-co-acrylic acid) P(NIPAAM-AA) polymer hydrogel, *J. Polym. Res.*, 2015, **22**, 33.

30 M. Franzreb, M. Siemann-Herzberg, T. J. Hobley and O. R. T. Thomas, Protein purification using magnetic adsorbent particles, *Appl. Microbiol. Biotechnol.*, 2006, **70**, 505–516.

31 M. Z. Sarker, M. M. Rahman, H. Minami, T. Suzuki, M. A. Rahman, A. Khan, S. M. Hoque and H. Ahmad, Magnetite incorporated amine-functional SiO_2 support for bimetallic Cu-Ni alloy nanoparticles produced highly effective nanocatalyst, *Colloids Surf., A*, 2022, **647**, 129044.

32 A. Rajan and N. K. Sahu, Review on magnetic nanoparticle-mediated hyperthermia for cancer therapy, *J. Nanopart. Res.*, 2020, **22**, 319.
33 A. Mukhatov, T.-A. Le, T. T. Pham and T. D. Do, A comprehensive review on magnetic imaging techniques for biomedical applications, *Nano Sel.*, 2023, **4**(3), 213–230.
34 C.-X. Zhao, L. Yu and A. P. J. Middelberg, Magnetic mesoporous silicananoparticles end-capped with hydroxyapatite for pH-responsive drug release, *J. Mater. Chem. B*, 2013, **1**(37), 4828–4833.
35 X. Tang, F. Jing, B. Lin, S. Cui, R. Yu, X. Shen and T. Wang, pH-responsive magnetic mesoporous silica-based nanoplatform for synergistic photodynamic therapy/chemotherapy, *ACS Appl. Mater. Interfaces*, 2018, **10**(17), 15001–15011.
36 S. Lai, H. Wang, N. Qiao, H. Shang, X. Sun, Z. Wang, Q. Li, Y. Lu and X. Zhang, Preparation and properties of pH-responsive magnetic mesoporous silica drug carrier, *J. Sol-Gel Sci. Technol.*, 2022, **103**, 139–150.
37 H. Keshavarz, A. Khavandi, S. Alamolhoda and M. R. Naimi-Jamal, pH-sensitive magnetic mesoporous silica nanocomposites for controlled drug delivery and hyperthermia, *RSC Adv.*, 2020, **10**(64), 39008–39016.
38 N. Avedian, F. Zaaeri, M. Daryasari, H. A. Javar and M. Khoobi, pH-sensitive biocompatible mesoporous magnetic nanoparticles labeled with folic acid as an efficient carrier for controlled anticancer drug delivery, *J. Drug Delivery Sci. Technol.*, 2018, **44**, 323–332.
39 Q. Zhao, P. Xie, X. Li, Y. Wang, Y. Zhang and S. Wang, Magnetic mesoporous silica nanoparticles mediated redox and pH dual-responsive target drug delivery for combined magnetothermal therapy and chemotherapy, *Colloids Surf., A*, 2022, **648**, 129359.
40 B. Chang, X. Sha, J. Guo, Y. Jiao, C. Wang and W. Yang, Thermo and pH dual responsive, polymer shell coated, magnetic mesoporous silicananoparticles for controlled drug release, *J. Mater. Chem.*, 2011, **21**(25), 9239–9247.
41 M. Tanjim, M. A. Rahman, M. M. Rahman, H. Minami, S. M. Hoque, M. K. Sharafat, M. A. Gafur and H. Ahmad, Mesoporous magnetic silica particles modified with stimuli-responsive P(NIPAM-DMA) valve for controlled loading and release of biologically active molecules, *Soft Matter*, 2018, **14**(26), 5469–5479.
42 T. Koltai, The pH paradigm in cancer, *Eur. J. Clin. Nutr.*, 2020, **74**, 14–19.
43 L. Liu, W. D. Yao, Y. F. Rao, X. Y. Lu and J. Q. Gao, pH-responsive carriers for oral drug delivery: challenges and opportunities for current platforms, *Drug Delivery*, 2017, **24**(1), 569–581.
44 S. Zhou, F. Zhang, J. Yu, X. Zhang, G. Yang and X. Liu, pH-sensitive biomaterials for drug delivery, *Molecules*, 2020, **25**(23), 5649.
45 T. Yoshida, T. C. Lai, G. S. Kwon and K. Sako, pH- and ion-sensitive polymers for drug delivery, *Expert Opin. Drug Delivery*, 2013, **10**(11), 1497–1513.
46 A. Ali, T. Aziz, J. Zheng, F. Hong, M. F. Awad, S. Manan, F. Haq, A. Ullah, M. N. Shah, Q. Javed, A. A. Kubar and L. Guo, Modification of cellulose nanocrystals with 2-carboxyethyl acrylate in the presence of epoxy resin for enhancing its adhesive properties, *Front. Bioeng. Biotechnol.*, 2022, **9**, 797672.
47 D. Lim, M.-J. Baek, H.-S. Kim, C. Baig and D. W. Lee, Carboxyethyl acrylate incorporated optically clear adhesives with outstanding adhesion strength and immediate strain recoverability for stretchable electronics, *Chem. Eng. J.*, 2022, **437**, 135390.
48 E. Pietrzak, P. Wiecinska and M. Szafran, 2-Carboxyethyl acrylate as a new monomer preventing negative effect of oxygen inhibition in gelcasting of alumina, *Ceram. Int.*, 2016, **42**(12), 13682–13688.
49 N. Ullah, F. Haq, A. Farid, M. Kiran, Z. A. Al Othman, A. M. Aljuwayid, M. A. Habila, A. Bokhari, S. Rajendran and K. S. Khoo, Coupling of carboxymethyl starch with 2-carboxyethyl acrylate: a new sorbent for the wastewater remediation of methylene blue, *Environ. Res.*, 2023, **219**, 115091.
50 N. A. Peppas and D. J. J. Am Ende, Controlled release of perfumes from polymers. II. Incorporation and release of essential oils from glassy polymers, *J. Appl. Polym. Sci.*, 1997, **66**(3), 509–513.
51 H. Ahmad, M. Nurunnabi, M. M. Rahman, K. Kumar, K. Tauer, H. Minami and M. A. Gafur, Magnetically doped multi stimuli-responsive hydrogel microspheres with IPN structure and application in dye removal, *Colloids Surf., A*, 2014, **459**, 39–47.
52 J. Nayeem, M. A. A. Al-Bari, M. Mahiuddin, M. A. Rahman, O. T. Mefford, H. Ahmad and M. M. Rahman, Silica coating of iron oxide magnetic nanoparticles by reverse microemulsion method and their functionalization with cationic polymer *P(NIPAm-co-AMPTMA)* for antibacterial vancomycin immobilization, *Colloids Surf., A*, 2021, **611**, 125857.
53 S. S. Ayoub, Paracetamol (acetaminophen): a familiar drug with an unexplained mechanism of action, *Temperature*, 2021, **8**(4), 351–371.
54 K. Do Kim, S. S. Kim, Y. H. Choa and H. T. Kim, Formation and surface modification of Fe_3O_4 nanoparticles by co-precipitation and sol-gel method, *J. Ind. Eng. Chem.*, 2007, **13**, 1137–1141.
55 G. Li, M. Liu, Z. Zhang, C. Geng, Z. Wu and X. Zhao, Extraction of methylmercury and ethylmercury from aqueous solution using surface sulfhydryl-functionalized mesoporous silica nanoparticles, *J. Colloid Interface Sci.*, 2014, **424**, 124–131.
56 S. S. Bristy, M. M. Rahman, M. M. Rahman, M. A. Alam, M. R. Karim and H. Ahmad, Epoxide functionalized γ-$Al_2O_3/Fe_3O_4/SiO_2$ nanocomposite and comparative adsorption behavior of a model reactive azo dye, *Int. J. Appl. Ceram. Technol.*, 2019, **16**(3), 1239–1252.
57 X. Li, H. Li, G. Liu, Z. Deng, S. Wu, P. Li and P. K. Chu, Magnetite-loaded fluorine-containing polymeric micelles for magnetic resonance imaging and drug delivery, *Biomaterials*, 2012, **33**(10), 3013–3024.

58 H. Ahmad, M. S. Rahman, M. A. J. Miah and A. M. I. Ali, A study on the production of PMMA/P(MMA-Aam) composite polymer particles and the effect of acrylamide content on the adsorption behaviors of biomolecules, *Colloid Polym. Sci.*, 2001, **279**(10), 1039–1043.

59 J. Rouquerol, D. Avnir, C. W. Fairbridge, D. H. Everett, J. M. Haynes, N. Pernicone and K. K. Unger, Recommendations for characterization of porous solids, *Pure Appl. Chem.*, 1994, **66**(8), 1739–1758.

60 B. L. F. Gleysteen and V. R. Deitz, Hysteresis in the physical adsorption of nitrogen on bone char and other adsorbents, *J. Res. Natl. Bur. Stand.*, 1945, **35**, 285–307.

61 V. T. Trinh, T. M. P. Nguyen, H. T. Van, L. P. Hoang, T. V. Nguyen, L. T. Ha, X. H. Vu, T. T. Pham, T. N. Quang and X. C. Nguyen, Phosphate adsorption by silver nanoparticles-loaded activated carbon derived from tea residue, *Sci. Rep.*, 2020, **10**, 3634.

62 B. Du, A. Mei, P. Tao, B. Zhao, Z. Cao, J. Nie and Z. Fan, Poly [*N*-isopropylacrylamide-*co*-3-(trimethoxysilyl)-propylmethacrylate] coated aqueous dispersed thermosensitive Fe_3O_4 nanoparticles, *J. Phys. Chem. C*, 2009, **113**(23), 10090–10096.

63 S. Hossain, M. Rahman, Y. Nahar, A. Rahman, M. K. Sharafat, M. Hossain and H. Ahmad, A simple in situ synthesis of iron oxide magnetic nanoparticles embedded in thermosensitive polymer for DNA capture, *J. Mater. Res.*, 2020, **35**(18), 2441–2450.

64 L. D. L. S. Valladares, L. L. Félix, S. E. Suarez, A. B. Dominguez, T. Mitrelias, S. Holmes and C. H. W. Barnes, Preparation and crystallization of hollow α-Fe_2O_3 microspheres following the gas-bubble template method, *Mater. Chem. Phys.*, 2016, **169**, 21–27.

65 H. B. Mohamed, S. M. El-Shanawany, M. A. Hamad and M. Elsabahy, Niosomes: a strategy toward prevention of clinically significant drug incompatibilities, *Sci. Rep.*, 2017, **7**, 6340.

66 J. P. Singhal and A. R. Ray, Synthesis of blood compatible polyamide block copolymers, *Biomaterials*, 2002, **23**(4), 1139–1145.